UNIVERSITY *of York*

This is a repository copy of *Voltage-controlled bimeron diode-like effect in nanoscale information channel*.

White Rose Research Online URL for this paper:
https://eprints.whiterose.ac.uk/id/eprint/206030/

Version: Published Version

Article:

White Rose
university consortium
Universities of Leeds, Sheffield & York

eprints@whiterose.ac.uk
https://eprints.whiterose.ac.uk/

PAPER • OPEN ACCESS

Voltage-controlled bimeron diode-like effect in nanoscale information channel

To cite this article: Gengxin Hu *et al* 2023 *J. Phys. D: Appl. Phys.* **56** 085001

View the article online for updates and enhancements.

Voltage-controlled bimeron diode-like effect in nanoscale information channel

Gengxin Hu[1,2,5]**, Jia Luo**[3,5]**, Junlin Wang**[2,*] **, Xianyang Lu**[1,*] **, Guoping Zhao**[3,*] **, Yuan Liu**[2]**, Jing Wu**[4] **and Yongbing Xu**[1,4,*]

[1] Jiangsu Provincial Key Laboratory of Advanced Photonic and Electronic Materials, School of Electronic Science and Engineering, Nanjing University, Nanjing 210093, People's Republic of China
[2] School of Integrated Circuits, Guangdong University of Technology, Guangzhou 510006, People's Republic of China
[3] College of Physics and Electronic Engineering, Sichuan Normal University, Chengdu 610068, People's Republic of China
[4] School of Physics, Engineering and Technology, University of York, York, YO10 5DD, United Kingdom

E-mail: junlin.wang@gdut.edu.cn, xylu@nju.edu.cn, zhaogp@uestc.edu.cn and ybxu@nju.edu.cn

CrossMark

Abstract
The magnetic bimeron, as the in-plane counterpart of the magnetic skyrmion, has potential applications in next-generation spin memory devices due to its lower energy consumption. In this work, the dynamic behavior of a current-driven bimeron in a nanotrack with voltage-controlled magnetic anisotropy (VCMA) is investigated. By adjusting the profile of the VCMA, the bimeron can display a diode-like unidirectional behavior in the nanotrack. The unidirectional behavior can be modulated by changing the driven current density and width of the VCMA region. The trajectory of the bimeron can also be controlled by the periodic VCMA region, which can enhance the stability of bimeron and realize a high-storage density bimeron-based information channel.

Supplementary material for this article is available online

(Some figures may appear in colour only in the online journal)

1. Introduction

With the development of information technology, traditional storage technology cannot meet the requirements of large capacity and high speed; consequently, high-performance storage technology is needed. Some high-performance storage schemes, such as magnetic domain walls and magnetic skyrmion-based racetrack memory are receiving extensive

attention due to very promising prospects for low-power memory and logic devices [1–6]. Magnetic skyrmions are nanoscale, particle-like topological configurations that have been found in chiral magnetic materials [7–11]. Compared with magnetic domain walls, skyrmions have greater potential due to their smaller size and lower critical current threshold [12, 13]. The bimeron is an in-plane topological counterpart of a magnetic skyrmion. The properties of magnetic bimerons and magnetic skyrmion have many similarities, such as the topological number, and they can be driven by spin-polarized current, spin waves, and anisotropy gradients [14–18]. Besides electric currents, skyrmions can be manipulated by various methods, such as spin waves, magnetic field gradients, magnetic anisotropy gradients, and temperature gradients [19–23]. The bimeron is stabilized by delicate competition between ferromagnetic exchange coupling, in-plane magnetic anisotropy

(IMA), and Dzyaloshinskii–Moriya interaction (DMI) in magnetic systems [24–30], while easy-plane magnetic anisotropy and shape anisotropy can also help the stabilization of the bimeron, owing to its in-plane spin texture [31, 32]. Compared with the skyrmion, magnetic bimerons have more interesting dynamics behavior which shows potential usage for microelectronics technology [33]. The bimeron is expected to serve as an information carrier in next-generation spin devices. Compared to skyrmions, bimerons exhibit some differences due to their asymmetric topology, which means they have high research significance.

Recently, some researchers have reported observation of the bimeron and the skyrmion in experiments [34, 35], and control of the skyrmion through voltage-controlled magnetic anisotropy (VCMA) [36]. Besides, the observation of domain wall bimerons [37] and transformation between bimeron and skyrmion has also been reported [38], which provides a good idea for spin topology to be used in storage applications. In this work, we report the dynamics behavior of the bimeron in a nanotrack channel with VCMA [39–41]. The study found that there is an anisotropy-current window in which the bimeron displays diode-like unidirectional motion behavior. Compared to skyrmion devices, the current-driven bimeron diode can be more easily driven, and the unidirectional motion behavior can be controlled by the magnitude of the drive current [42–45]. The bimeron's controllable one-way trafficability makes it possible to have more applications. This phenomenon can facilitate the construction of a bimeron diode-effect information channel. Additionally, the dynamics behavior of the bimeron with the different driven current density and different profiles of the VCMA region is studied. The results show that the trajectory of the bimeron can be modulated by the different profiles of the VCMA region [46, 47]. This will contribute to the development of the bimeron storage channel, for application in information storage technology.

2. Model and simulation

The simulation model is an ultra-thin ferromagnetic nanotrack, $1000 \times 200 \times 0.4$ nm, as shown in figure 1(b). The model is discretized into a rectangular cell with a volume of $4 \times 4 \times 0.4$ nm. All the micromagnetic simulations in this paper are provided by the object oriented micromagnetic framework (OOMMF) [48]. The fundamentals of micromagnetic simulation are described by the Landau–Lifshitz-Gilbert (LLG) equation, which is written as

$$\frac{d\boldsymbol{m}}{dt} = -\gamma_0 \boldsymbol{m} \times h_{\text{eff}} + \alpha \left(\boldsymbol{m} \times \frac{d\boldsymbol{m}}{dt} \right) - \mu \boldsymbol{m} \times (\boldsymbol{m} \times \boldsymbol{p}), \quad (1)$$

where $\boldsymbol{m}$ stands for the reduced magnetization $\boldsymbol{M}/Ms$ where Ms is the saturation magnetization. The damping coefficient and the absolute value of the gyromagnetic ratio are described by γ_0 and α, respectively. $\boldsymbol{h}_{\text{eff}}$ is the effective field, including the contributions of exchange, DMI, IMA, and demagnetization. The parameter μ represents the $\frac{\gamma_0 \hbar j \theta SH}{2 t_z e \mu_0 M_S}$, where $\hbar$ is the reduced Plank constant, j is the applied current density, $\theta_{\text{SH}} = 0.08$ and

represents the spin Hall angle, e is the electron charge, μ_0 is the vacuum permeability constant, and t_z is the thickness of the magnetic nanotrack [49]. $\boldsymbol{p}$ is the direction of the spin polarization. The other parameters in the micromagnetic simulation refer to [50]: the saturation magnetization $Ms = 580$ kA m^{-1}, the damping coefficient $\alpha = 0.1$, the DMI constant D is chosen as $D = 2.9$ mJ m^{-2}, and the exchange constant $A = 14$ pJ m^{-1}. The applied current is spin-orbit torque (SOT) current, and the current polarization direction is along the $+z$ direction. In addition to the parameters for the LLG equation, the profile of the VCMA in the nanotrack is shown in figure 1(c). The VCMA is a slope profile that varies linearly between K_{u0} and K_{uv}, and schematic diagram is shown in figure 1(a). There are two kinds of slope profile used in the simulation. The function for the slope x profile is given as:

$$Ku(x) = Ku0 + \frac{Kuv - Ku0}{w}(x - start)(start \leqslant x \leqslant w + start), \quad (2)$$

$$Ku(x) = Kuv - \frac{Kuv - Ku0}{w}(x - start)(start \leqslant x \leqslant w + start), \quad (3)$$

where w is the period length, *start* is the start point of the profile change, K_{u0} is the original value of the VCMA, and K_{uv} is the maximum value of the VCMA. The sharp anisotropy profile can be realized in a thickness gradient along an x-axis of magnetic multi-layers [51] or engineered by irradiating the strip with gallium ions (Ga+) of varying intensity [2]. The shape of the profile is changed when studying the dynamics behavior of the bimeron under different periodic VCMA regions. The profile of the period VCMA region is given as:

$$Ku(x) = Ku0 + \frac{Kuv - Ku0}{2}(1 + \sin(2\pi x/w)), \quad (4)$$

where the parameter definitions are consistent with equation (2). The profile is shown in figure 1(d).

In the simulation, the bimeron initial position is on the left side of the nanotrack with the topological number $Q = -1$. The definition of topological number is shown in supplementary material figure S1. The bimeron with asymmetric topology structure can be driven by the spin-polarized current. It has been found that the bimeron with $Q = -1$ can stably move to the right side of the channel when it is driven by a spin-polarized current which is polarized along the $+z$ axis. However, if the bimeron is driven by the opposite spin current along the $+z$ axis, the stability of the bimeron is greatly reduced and the bimeron will be destroyed. The bimeron's symmetry along the y- *axis* is studied, and the results are given in supplementary material figure S2. Its movement driven by the current is shown in supplementary material figure S3.
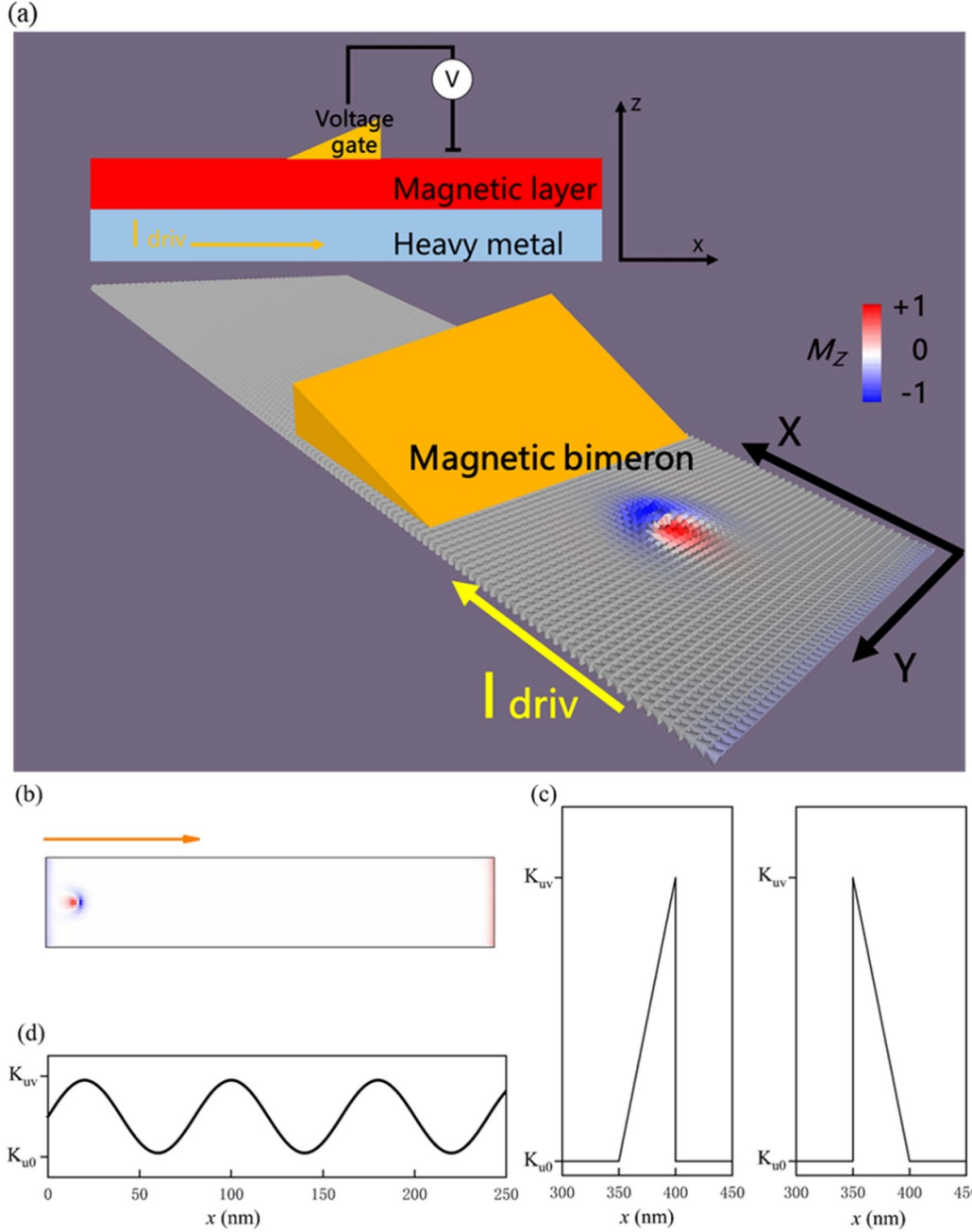
Figure 1. (a) Illustration of the bimeron diode device controlled by a gate voltage. The out-of-plane magnetization component (m_z) is color coded: red means $m_z = +1$, white means $m_z = 0$, and blue means $m_z = -1$. The background magnetization is $m_x = +1$. I_{driv} means driven current. (b) A schematic of the ferromagnetic nanotrack where a magnetic bimeron is initially placed on the left and right, respectively. (c) A linear anisotropy profile. (d) The profile of the period externally VCMA region, gentle slope and steep slope, respectively.

3. Results and discussion

3.1. The pass/broken states of an isolated bimeron in the nanotrack

The profile of the slope-shaped VCMA region is shown in figure 1(c). The VCMA region can be realized by the VCMA effect and wedge-shaped magnetic thin film [52]. The magnetic anisotropy fields for the two variation trends are defined as gentle slope and steep slope, respectively. The starting positions of the applied external fields are all at $x = 300$ nm. In the

simulation, the influence of the VCMA region on the dynamics behavior of the current-driven bimeron is mainly studied. When a bimeron goes through the VCMA region, it will show two motion states; in one it passes through the VCMA region, and in the other it is destroyed in the VCMA region, which are defined as PASS and BROKEN states, respectively. However, due to the opposite variation trend of the VCMA profiles, the final state of bimerons going through the VCMA region is different.

By adjusting the K_{uv} and w of the VCMA region, the simulation is carried out under a current density j of 55.0, 57.5,
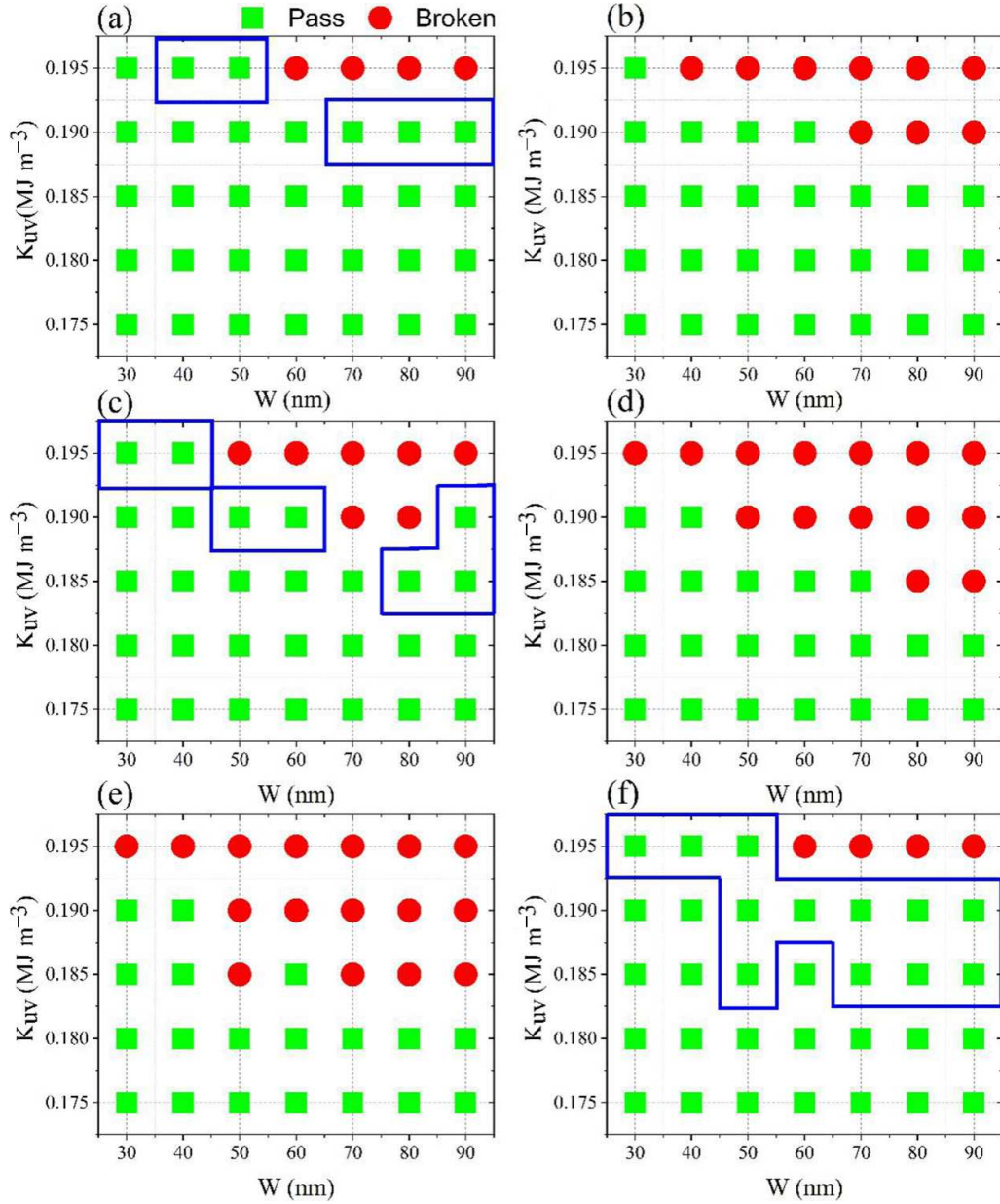
Figure 2. The pass/broken states of a bimeron driven by spin current in a ferromagnetic nanotrack. The pass/broken states of the bimeron at various values of *w* and K_{uv}, where the trend of slope variation is (a) gentle slope and (b) steep slope, and the current density *j* is 55.0 MA cm^{-2}. (c) and (d) are with the same conditions as (a) and (b), but the current density is 57.5 MA cm^{-2}. (e) and (f) are with the same conditions as (a) (b), but the current density is 60.0 MA cm^{-2}.

and 60.0 MA cm^{-2}, and the results of the final state of bimerons entering the VCMA region are given in figure 2. In the phase diagram, it can be seen that, whether the bimeron goes through the gentle slope or steep slope, it will be destroyed in the nanotrack when the values of K_{uv} and *w* are too large. In addition, the variation trend of the VCMA region also affects the dynamics behavior of bimerons in the VCMA region.

When the current-driven magnetic bimerons move toward the right side of the nanowire in the slope region, the larger current density will induce bimerons to break more easily at the VCMA region. But for the anti-slope VCMA region, the large current density is beneficial for bimerons going through the VCMA region. In the fixed driven current density, the final state of bimerons going through the VCMA region will be influenced by changing the K_{uv} and *w* of the VCMA region. For a VCMA region with two variation trends at the same K_{uv} and *w*, bimerons may exhibit different dynamic properties. When *j* = 55.0 MA cm^{-2} for the slope of the VCMA region, with K_{uv} = 0.195 MJ m^3 and a range of 40–50 nm for *w*, the bimeron can pass through the VCMA region, and correspondingly, under same K_{uv} and *w* but a steep slope, the bimeron will break in the VCMA region. By adjusting the variation trend of the VCMA region, the same bimeron can show unidirectional behavior when passing through the VCMA region. Besides this, for the cases of *j* = 57.5 MA cm^{-2} and *j* = 60.0 MA cm^{-2}, there is are also parameter conditions which allow this
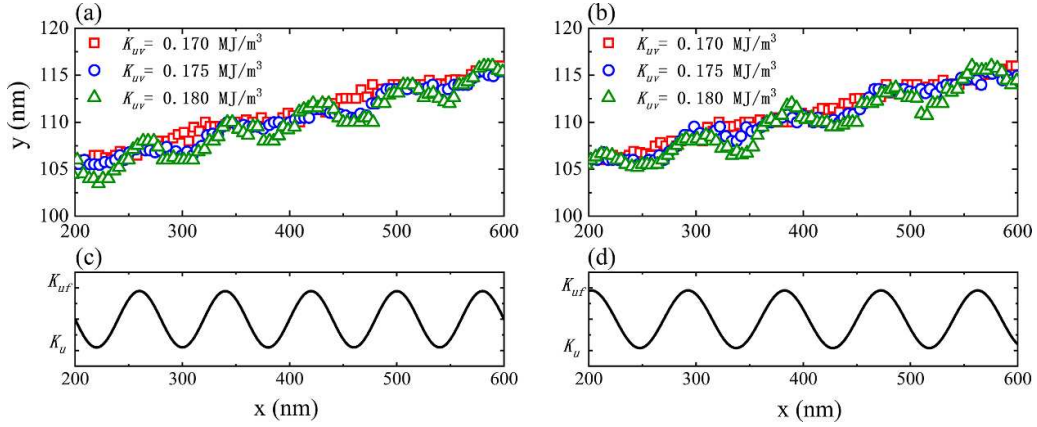
Figure 3. The trajectory diagram, (a) and (b), of the bimeron in a periodic VCMA region. The profile of the corresponding fields, as figure 1(c), are shown in (c) and (d). The current j is 50.0 MA cm^{-2}. In (a) and (c), the value of w is 80 nm, and in (b) and (d) it is 90 nm.

unidirectional behavior. Such parameter conditions are marked with a blue box in figure 2.

In addition to variation trend in the VCMA region, driven current density also affects the dynamics behavior of bimerons. It is found that when the current density is small, it is easier for the bimeron to go through the gentle-slope VCMA region. If the VCMA region has a steep slope, it will block thebimeron going through the VCMA region. After increasing the driven current density to 57.5 MA cm^{-2}, the two types of slope for the VCMA region showed no tendency to block bimeron. Under the same conditions, the behavior of bimerons passing through the differently shaped VCMA regions are the same. However, variation in the VCMA slope can make certain conditions passable with a gentle slope and impassable with a steep slope, and vice versa. On increasing the driven current density to 60.0 MA cm^{-2}, it is found that there is a larger parameter window that allows bimerons to pass through the steep slope. According to the unidirectional motion behavior, it shows that the VCMA region is easy for bimerons to pass through the steep slope, although they break with the gentle slope.

By adjusting the K_{uv} and w of the VCMA region, the dynamics behavior can be modulated by changing the profile of the VCMA region. For the same parameter combination of K_{uv} and w, while the bimeron goes through the VCMA region, the influence of the different shapes of VCMA region on the bimeron is different. By choosing an appropriate combination of parameters, the bimeron will show one-way passability for VCMA on gentle or steep slopes, which can be used for the construction of a bimeron diode. Variation in the driven current density also affects the dynamic properties of the bimeron in the VCMA region. When the driven current is small, the VCMA region with a gentle slope is easier for bimeron to pass through, and when the current is large, the VCMA region with a steep slope is easier for bimeron to pass through. In particular, for a given combination of K_{uv} and w for a VCMA region, by changing the driven current density, the bimeron may change from one-way traffic on a gentle slope to one-way

traffic on a steep slope, or vice versa. This shows that the unidirectional behavior of the bimeron in the VCMA region is affected not only by the profile of the VCMA but also by the driven current density. Therefore, there is a parameter window that can be used to build a bimeron-based diode. By changing the driven current density and the shape of the VCMA region, the bimerons in the nanotrack can achieve unidirectional movement. However, the thermal fluctuation in the system will reduce the effect of anisotropy and reduce the stability of the spin topology [53]. In this work, we only consider the system without a thermal effect. The negative effect from thermal fluctuation can be reduced by choosing a high Curie temperature material.

3.2. Bimeron motion with a periodic sine-type VCMA region on the nanotrack

Similar to skyrmions, bimerons also have the skyrmion Hall effect, and there is a phenomenon of moving toward the edge of the channel driven by the spin current. By increasing the magnetic anisotropy in the region, the longitudinal velocity of the skyrmion can be reduced, and the effect of weakening the skyrmion hall effect (SKHE) of the skyrmion can be achieved. Therefore, to study the effect of a periodically varying VCMA region on the dynamic properties of the bimeron, the dynamic properties of the bimeron under the effect of an external field were studied by applying a periodic sin-type VCMA region on the nanotrack. The profile of the VCMA region is shown in the experimental section. The trajectory diagram of the bimeron is shown in figure 3.

When there is no VCMA region, the trajectory of the bimeron appears as an inclined straight line. This is because the bimeron is driven by the Magnus force, so the bimeron will show the characteristics of vertical motion. When a sine-type VCMA region is applied to the nanotrack, the trajectory of the bimeron also changes. Comparing the trajectory of the bimeron with the shape of the VCMA region, the trajectory of bimeron shows the same shape as the VCMA, but the
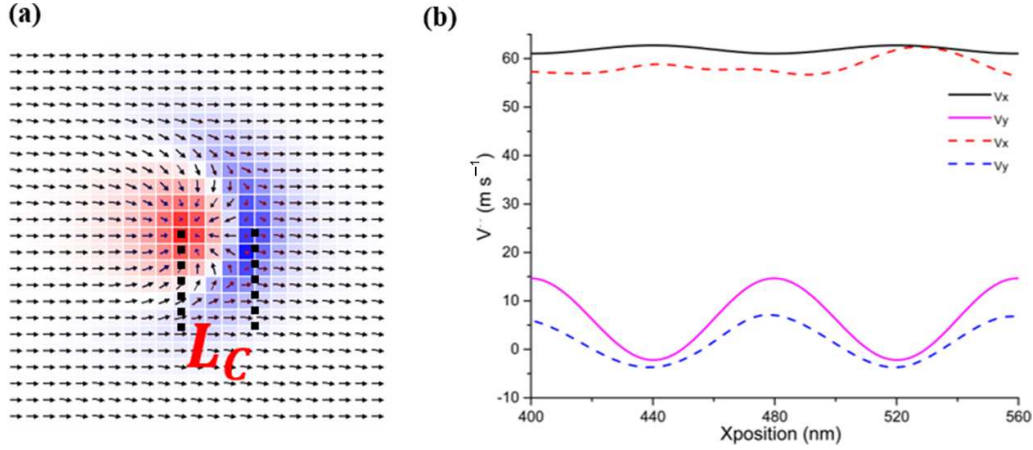
J. Phys. D: Appl. Phys. **56** (2023) 085001

G Hu *et al*

Figure 4. (a) Bimeron magnetization distribution. The colors represent the component of the magnetization on the *z*-axis (red is positive, blue is negative), and the arrows represent the projection of the magnetization on the *xoy*-plane. (b). Velocity curve of an ferromagnetic (FM) bimeron. The solid line is the analytical solution, and the dashed line is the numerical result. The horizontal axis is the *x*-position (nm), and the vertical axis is the speed (m s^{-1}).

phase is delayed. The trajectory of the bimeron will appear as a slanted straight line under the trajectory obtained without the VCMA region, showing the regulation of the bimeron trajectory by the VCMA. The K_{uv} value of the VCMA also affects the bimeron trajectory. The larger the K_{uv} value, the more the bimeron's trajectory follows the sine wave. The VCMA will affect the speed of the bimeron, and finally, the motion trajectory of the bimeron will change relative to when there is no VCMA region. After applying a sine-type VCMA region, when the VCMA increases, the longitudinal velocity of the bimeron will decrease, so the overall trajectory of the bimeron will appear below the motion trajectory obtained without the external field. Since the changing external field directly affects the velocity of the bimeron, although its trajectory also shows a sine shape similar to that of the VCMA, the change will have a certain delay relative to the speed change, and the overall trajectory of the bimeron will show phase delay characteristics. The larger the value of the applied VCMA region, the larger the influence on the speed of the bimeron, the greater the change in the bimeron's speed when the speed changes, and the greater the distance of upward or downward movement.

Therefore, for a current-driven bimeron, the motion of the bimeron can be adjusted by changing the magnetic anisotropy in the specific area so that the bimeron can overcome the adverse effects brought by the SKHE during the moving process. The bimeron will not move all the way toward the edge of the channel but will show the opposite movement trend sometimes. By choosing the appropriate value of the external field, the motion of the bimeron can be adjusted, and the stability of the bimeron topology can be ensured, which provides an important idea for the development of bimeron information storage technology.

3.3. Comparison between the theoretical speed and the simulation speed of a bimeron

Specifically, we calculated the speed of a bimeron with $w = 80$ and $K_{uv} = 0.18$ by measuring the displacement of the bimeron

over a period of time. The theoretical speed is calculated after derivation of an equation. The speed in the actual simulation is calculated according to the trajectory of the bimeron. The bimeron can be regarded as a rigid particle as the changes due to the magnet anisotropy gradient in its diameter and cycloid length (L_C is the length from $mz = 1$ to -1, see figure 4(a)) are small. Therefore, the steady motion of a rigid bimeron can be well described by the Thiele motion equation, which is expressed as follows [54, 55]:

$$\boldsymbol{G} \times \boldsymbol{v} - \alpha \boldsymbol{D} \cdot \boldsymbol{v} - \boldsymbol{F}_j - \boldsymbol{F}_K = 0. \tag{5}$$

The first term on the left side of equation (5) is the Magnus force term with the gyromagnetic coupling vector $\boldsymbol{G} = (4\pi Q \mu_0 \mathrm{M}_s t_z/\gamma_0) \, \boldsymbol{e}_z$ where the skyrmion number Q of the isolated FM bimeron is ± 1 [56, 57], and the other parameters are: the velocity of bimeron $\boldsymbol{v}$, the damping coefficient α, the vacuum permeability constant μ_0, the saturation magnetization M_s, the ferromagnetic layer thickness t_z, the gyromagnetic ratio γ_0, and the Z-axis unit vector e_z. The second term on the left side of equation (5) is the dissipative force term with the dissipative tensor describing the effect of the dissipative force on the moving magnetic skyrmion $\boldsymbol{D} = (\mu_0 M_s t_z/\gamma_0) \begin{pmatrix} d & 0 \\ 0 & d \end{pmatrix}$ where the tensor components are calculated by $d = \int (\partial_x \boldsymbol{m} \cdot \partial_x \boldsymbol{m}) \, \mathrm{d}x \mathrm{d}y$. The third term on the left side of equation (5) is the driving force term with the tensor generated by $\boldsymbol{F}_j = (\mu_0 B_j M_s t_z/\gamma_0) \begin{pmatrix} I_x \\ I_y \end{pmatrix}$, where B_j relates to the applied current density j, defined as $B_j = \gamma_0 \hbar \theta_{\mathrm{SH}} j / 2\mu_0 e t_z M_s$ with the reduced Plank constant $\hbar$, the spin hall angle θ_{SH}. The tensor components are calculated by $I_i = \int [(m \times p) \cdot \partial_i m] \, \mathrm{d}x \mathrm{d}y$. The fourth term $\boldsymbol{F}_K$ on the left side of equation (5) is the force which is related to the magnetic anisotropy gradient, and can be defined as $\boldsymbol{F}_K = \int (\partial U/\partial r) \, \mathrm{d}x \mathrm{d}y$ [21, 55]. The potential energy U of the system contains the exchange energy,

J. Phys. D: Appl. Phys. **56** (2023) 085001

G Hu *et al*

DMI energy, anisotropy energy, and dipole-dipole interaction (DDI) energy, which is written as follows [57–59]:

$$U = \int \left\{ A(\nabla \boldsymbol{m})^2 + D_{\mathrm{MI}} \left[m_z \nabla \cdot \boldsymbol{m} - (\boldsymbol{m} \cdot \nabla) m_z \right] \right. $$
$$\left. - K m_x^2 - \mu_0 M_S \boldsymbol{H_d} \cdot \boldsymbol{m} \right\} dV. \tag{6}$$

where A, D, K, and $\boldsymbol{H}_d$ represent the Heisenberg exchange constant, DM interaction constant, the magnetic anisotropy constant, and the demagnetization field, respectively. Solving equation (6), the velocity of the bimeron without boundary effect can be obtained,

$$v_x = -\frac{\alpha d (B_j I_x + v_K) - 4\pi Q B_j I_y}{(4\pi Q)^2 + \alpha^2 d^2}; \tag{7a}$$

$$v_y = -\frac{4\pi Q (B_j I_x + v_K) + \alpha d B_j I_y}{(4\pi Q)^2 + \alpha^2 d^2}, \tag{7b}$$

where $v_K = \frac{\gamma}{\mu_0 M_S t_z} \int \frac{\partial K}{\partial x} \cos^2 \theta \mathrm{d}V$. According to [44], $I_x = 0$, $I_y \approx \pi^2 L_C / 2$, and $d \approx 2\pi \left(\frac{L_C}{2\sqrt{\frac{A}{K}}} + \frac{2\sqrt{\frac{A}{K}}}{L_C} \right)$, where $L_C \approx$ 16 nm, $d \approx 2\pi$, and $Q = -1$.

As presented in figure 4(b), when $K = K_{u0} + \frac{K_{uv} - K_{u0}}{2} \left[1 + \sin \left(\frac{2\pi x}{w} \right) \right]$ with $K_{u0} = 0.17$ MJ m^{-3}, $K_{uv} = 0.18$ MJ m^{-3}, and period length $w = 80$ nm, the velocity of a FM bimeron can be solved analytically, and the images compared with the simulation results are shown in figure 4(b). It can be seen from figure 4(b) that the velocities in the x and y directions both fluctuate periodically with the position, and the influence of v_x is small, while that of v_y is very large. We found that the two are in good agreement overall, but with larger velocity deviations in the y-direction. This is reasonable because the analytical solution does not consider the boundary effect. In the simulation, when the bimeron approaches the boundary, there will be a force opposite to the direction of the velocity, which will shift the velocity in the y-direction. The y-component velocity of the bimeron is oscillatory around 0 due to the distribution of the VCMA region. Mostly, the bimeron has a y-component velocity larger than 0 which makes the bimeron trajectory move toward the $+y$ direction. The theoretical velocity calculation from the Thiele motion equation is in good agreement with the results from micromagnetic simulation.

4. Conclusion

In summary, the dynamics behavior of the bimeron investigated by OOMMF simulation is in good agreement with the theoretical calculation. After adding VCMA inside the nanotrack, the dynamics behavior of the bimeron when passing through sloped VCMA is investigated. The research shows that when VCMA is too large the dbimeron is destroyed. More importantly, for a specific profile of VCMA, the bimeron shows unidirectional behavior when passing through different slopes. This unidirectional behavior is not only related to the profile of the VCMA but also affected by the driven current density.

For a VCMA region with a certain combination of parameters, the bimeron can show both gentle-slope pass and steep-slope pass, which can be achieved by adjusting the driven current density. This allows bimeron-based diodes to exhibit tunable unidirectional behavior. On the other hand, by adding a periodic, sine-type VCMA to the nanotrack, the trajectory of the bimeron can be well modulated. By increasing the magnetic anisotropy in a specific area, the longitudinal velocity of the bimeron can be adjusted, and the SKHE of the bimeron can be weakened to a certain extent so that when the bimeron moves in the nanotrack, it can avoid topological damage caused by the movement to the edge of the channel.

Data availability statement

The data that support the findings of this study are available upon reasonable request from the authors.

ORCID iDs

Junlin Wang https://orcid.org/0000-0002-0383-7864
Xianyang Lu https://orcid.org/0000-0003-3815-4032
Guoping Zhao https://orcid.org/0000-0002-3327-9445

References

[1] Han N M, Guo G H, Zhang G F, Song W B and Men G F 2007 Domain wall structure transition during magnetization reversal process in magnetic nanowires *Trans. Nonferr. Met. Soc. China* **17** 1034–7
[2] Franken J H, Swagten H J M and Koopmans B 2012 Shift registers based on magnetic domain wall ratchets with perpendicular anisotropy *Nat. Nanotechnol.* **7** 499–503
[3] Franken J, Yin Y, Schellekens A, van den Brink A, Swagten H and Koopmans B 2013 Voltage-gated pinning in a magnetic domain-wall conduit *Appl. Phys. Lett.* **103** 102411–4
[4] Ummelen F, Swagten H and Koopmans B 2017 Racetrack memory based on in-plane-field controlled domain-wall pinning *Sci. Rep.* **7** 1–8

J. Phys. D: Appl. Phys. **56** (2023) 085001

G Hu *et al*

[5] Li Z D, Hu Y C, He P B and Sun L L 2018 Domain wall dynamics in magnetic nanotubes driven by an external magnetic field *Chin. Phys.* B **27** 077505

[6] Zhao Z X, He P B, Cai M Q and Li Z D 2020 Spin waves and transverse domain walls driven by spin waves: role of damping *Chin. Phys.* B **29** 077502

[7] Pfleiderer C, Adams T, Bauer A, Biberacher W, Binz B, Birkelbach F, Böni P, Franz C, Georgii R and Janoschek M 2010 Skyrmion lattices in metallic and semiconducting B20 transition metal compounds *J. Phys.: Condens. Matter* **22** 164207

[8] Münzer W, Neubauer A, Adams T, Mühlbauer S, Franz C, Jonietz F, Georgii R, Böni P, Pedersen B and Schmidt M 2010 Skyrmion lattice in the doped semiconductor Fe$_{1-x}$Co$_x$ Si *Phys. Rev.* B **81** 041203

[9] Yu X, Kanazawa N, Onose Y, Kimoto K, Zhang W, Ishiwata S, Matsui Y and Tokura Y 2011 Near room-temperature formation of a skyrmion crystal in thin-films of the helimagnet FeGe *Nat. Mater.* **10** 106–9

[10] Heinze S, Von Bergmann K, Menzel M, Brede J, Kubetzka A, Wiesendanger R, Bihlmayer G and Blügel S 2011 Spontaneous atomic-scale magnetic skyrmion lattice in two dimensions *Nat. Phys.* **7** 713–8

[11] Seki S, Yu X, Ishiwata S and Tokura Y 2012 Observation of skyrmions in a multiferroic material *Science* **336** 198–201

[12] Zhang X, Zhao G, Fangohr H, Liu J P, Xia W, Xia J and Morvan F 2015 Skyrmion-skyrmion and skyrmion-edge repulsions in skyrmion-based racetrack memory *Sci. Rep.* **5** 1–6

[13] Kang W, Zheng C, Huang Y, Zhang X, Zhou Y, Lv W and Zhao W 2016 Complementary skyrmion racetrack memory with voltage manipulation *IEEE Electron Device Lett.* **37** 924–7

[14] Nagaosa N and Tokura Y 2013 Topological properties and dynamics of magnetic skyrmions *Nat. Nanotechnol.* **8** 899–911

[15] Fert A, Cros V and Sampaio J 2013 Skyrmions on the track *Nat. Nanotechnol.* **8** 152–6

[16] Yu X, Tokunaga Y, Kaneko Y, Zhang W, Kimoto K, Matsui Y, Taguchi Y and Tokura Y 2014 Biskyrmion states and their current-driven motion in a layered manganite *Nat. Commun.* **5** 1–7

[17] Du H, DeGrave J P, Xue F, Liang D, Ning W, Yang J, Tian M, Zhang Y and Jin S 2014 Highly stable skyrmion state in helimagnetic MnSi nanowires *Nano Lett.* **14** 2026–32

[18] Du H, Che R, Kong L, Zhao X, Jin C, Wang C, Yang J, Ning W, Li R and Jin C 2015 Edge-mediated skyrmion chain and its collective dynamics in a confined geometry *Nat. Commun.* **6** 1–7

[19] Zhang X, Ezawa M, Xiao D, Zhao G, Liu Y and Zhou Y 2015 All-magnetic control of skyrmions in nanowires by a spin wave *Nanotechnology* **26** 225701

[20] Liang J, Yu J, Chen J, Qin M, Zeng M, Lu X, Gao X and Liu J M 2018 Magnetic field gradient driven dynamics of isolated skyrmions and antiskyrmions in frustrated magnets *New J. Phys.* **20** 053037

[21] Shen L, Xia J, Zhao G, Zhang X, Ezawa M, Tretiakov O A, Liu X and Zhou Y 2018 Dynamics of the antiferromagnetic skyrmion induced by a magnetic anisotropy gradient *Phys. Rev.* B **98** 134448

[22] Khoshlahni R, Qaiumzadeh A, Bergman A and Brataas A 2019 Ultrafast generation and dynamics of isolated skyrmions in antiferromagnetic insulators *Phys. Rev.* B **99** 054423

[23] Ye C, Li L L, Shu Y, Li Q, Xia J, Hou Z, Zhou Y, Liu X, Yang Y and Zhao G 2022 Generation and manipulation of skyrmions and other topological spin structures with rare metals *Rare Met.* **41** 1–17

[24] Jiang W, Upadhyaya P, Zhang W, Yu G, Jungfleisch M B, Fradin F Y, Pearson J E, Tserkovnyak Y, Wang K L and Heinonen O 2015 Blowing magnetic skyrmion bubbles *Science* **349** 283–6

[25] Kim S K 2019 Dynamics of bimeron skyrmions in easy-plane magnets induced by a spin supercurrent *Phys. Rev.* B **99** 224406

[26] Göbel B, Mook A, Henk J, Mertig I and Tretiakov O A 2019 Magnetic bimerons as skyrmion analogues in in-plane magnets *Phys. Rev.* B **99** 060407

[27] Li X, Shen L, Bai Y, Wang J, Zhang X, Xia J, Ezawa M, Tretiakov O A, Xu X and Mruczkiewicz M 2020 Bimeron clusters in chiral antiferromagnets *npj Comput. Mater.* **6** 1–9

[28] Shen L, Li X, Xia J, Qiu L, Zhang X, Tretiakov O A, Ezawa M and Zhou Y 2020 Dynamics of ferromagnetic bimerons driven by spin currents and magnetic fields *Phys. Rev.* B **102** 104427

[29] Zhang X, Xia J, Shen L, Ezawa M, Tretiakov O A, Zhao G, Liu X and Zhou Y 2020 Static and dynamic properties of bimerons in a frustrated ferromagnetic monolayer *Phys. Rev.* B **101** 144435

[30] Shen L, Xia J, Zhang X, Ezawa M, Tretiakov O A, Liu X, Zhao G and Zhou Y 2020 Current-induced dynamics and chaos of antiferromagnetic bimerons *Phys. Rev. Lett.* **124** 037202

[31] Jiang J, Liu X, Li R and Mi W 2021 Topological spin textures in a two-dimensional MnBi$_2$(Se, Te)$_4$ Janus material *Appl. Phys. Lett.* **119** 072401

[32] Silva R, Silva R, Moura-Melo W and Pereira A 2022 Skyrmion dynamics and skyrmion–bimeron crossover in antiferromagnetic thin nanodisks with a random distribution of magnetic impurities *J. Magn. Magn. Mater.* **546** 168823

[33] Göbel B, Mertig I and Tretiakov O A 2021 Beyond skyrmions: review and perspectives of alternative magnetic quasiparticles *Phys. Rep.* **895** 1–28

[34] Yu X, Koshibae W, Tokunaga Y, Shibata K, Taguchi Y, Nagaosa N and Tokura Y 2018 Transformation between meron and skyrmion topological spin textures in a chiral magnet *Nature* **564** 95–98

[35] Tran B X, Yang S, Kim H J, Ha J H, Yoon S, Kim C, Moon K W, Choi W C, Hwang C and Hong J I 2022 Electrical manipulation of oxygen ion migrations for the voltage-controlled adjustment of magnetic anisotropy and optimized skyrmion generations *Adv. Electron. Mater.* **8** 2200770

[36] Zhou Y, Mansell R and van Dijken S 2021 Voltage control of skyrmions: creation, annihilation, and zero-magnetic field stabilization *Appl. Phys. Lett.* **118** 172409

[37] Nagase T, So Y-G, Yasui H, Ishida T, Yoshida H K, Tanaka Y, Saitoh K, Ikarashi N, Kawaguchi Y and Kuwahara M 2021 Observation of domain wall bimerons in chiral magnets *Nat. Commun.* **12** 1–8

[38] Ohara K, Zhang X, Chen Y, Kato S, Xia J, Ezawa M, Tretiakov O A, Hou Z, Zhou Y and Zhao G 2022 Reversible transformation between isolated skyrmions and bimerons *Nano Lett.* **22** 8559–66

[39] Wang J, Xia J, Zhang X, Zhao G, Ye L, Wu J, Xu Y, Zhao W, Zou Z and Zhou Y 2018 Controllable transport of a skyrmion in a ferromagnetic narrow channel with voltage-controlled magnetic anisotropy *J. Phys. D: Appl. Phys.* **51** 205002

[40] Zhao L, Liang X, Xia J, Zhao G and Zhou Y 2020 A ferromagnetic skyrmion-based diode with a voltage-controlled potential barrier *Nanoscale* **12** 9507–16

[41] Shu Y, Li Q, Xia J, Lai P, Hou Z, Zhao Y, Zhang D, Zhou Y, Liu X and Zhao G 2022 Realization of the skyrmionic logic gates and diodes in the same racetrack with enhanced and modified edges *Appl. Phys. Lett.* **121** 042402

[42] Wang J, Xia J, Zhang X, Zheng X, Li G, Chen L, Zhou Y, Wu J, Yin H and Chantrell R 2020 Magnetic skyrmionium

J. Phys. D: Appl. Phys. **56** (2023) 085001

G Hu *et al*

diode with a magnetic anisotropy voltage gating *Appl. Phys. Lett.* **117** 202401

[43] Jung D-H, Han H-S, Kim N, Kim G, Jeong S, Lee S, Kang M, Im M-Y and Lee K-S 2021 Magnetic skyrmion diode: unidirectional skyrmion motion via symmetry breaking of potential energy barriers *Phys. Rev.* B **104** L060408

[44] Song L, Yang H, Liu B, Meng H, Cao Y and Yan P 2021 A spin-wave driven skyrmion diode under transverse magnetic fields *J. Magn. Magn. Mater.* **532** 167975

[45] Feng Y, Zhang X, Zhao G and Xiang G 2022 A skyrmion diode based on skyrmion hall effect *IEEE Trans. Electron Devices* **69** 1293–7

[46] Xia J, Zhang X, Ezawa M, Shao Q, Liu X and Zhou Y 2020 Dynamics of an elliptical ferromagnetic skyrmion driven by the spin–orbit torque *Appl. Phys. Lett.* **116** 022407

[47] Göbel B, Mook A, Henk J and Mertig I 2019 Overcoming the speed limit in skyrmion racetrack devices by suppressing the skyrmion Hall effect *Phys. Rev.* B **99** 020405

[48] Donahue M J and Donahue M J 1999 OOMMF user's guide (available at: https://math.nist.gov/oommf/)

[49] Woo S, Song K M, Han H-S, Jung M-S, Im M-Y, Lee K-S, Song K S, Fischer P, Hong J-I and Choi J W 2017 Spin-orbit torque-driven skyrmion dynamics revealed by time-resolved x-ray microscopy *Nat. Commun.* **8** 1–8

[50] Wiesendanger R 2016 Nanoscale magnetic skyrmions in metallic films and multilayers: a new twist for spintronics *Nat. Rev. Mater.* **1** 1–11

[51] Ma C, Zhang X, Xia J, Ezawa M, Jiang W, Ono T, Piramanayagam S, Morisako A, Zhou Y and Liu X 2018 Electric field-induced creation and directional motion of domain walls and skyrmion bubbles *Nano Lett.* **19** 353–61

[52] Xia J, Huang Y, Zhang X, Kang W, Zheng C, Liu X, Zhao W and Zhou Y 2017 A microwave field-driven transistor-like skyrmionic device with the microwave current-assisted skyrmion creation *J. Appl. Phys.* **122** 153901

[53] Tomasello R, Guslienko K, Ricci M, Giordano A, Barker J, Carpentieri M, Chubykalo-Fesenko O and Finocchio G 2018 Origin of temperature and field dependence of magnetic skyrmion size in ultrathin nanodots *Phys. Rev.* B **97** 060402

[54] Thiele A A 1973 Steady-state motion of magnetic domains *Phys. Rev. Lett.* **30** 230

[55] Shen L, Xia J, Zhao G, Zhang X, Ezawa M, Tretiakov O A, Liu X and Zhou Y 2019 Spin torque nano-oscillators based on antiferromagnetic skyrmions *Appl. Phys. Lett.* **114** 042402

[56] Murooka R, Leonov A O, Inoue K and Ohe J-I 2020 Current-induced shuttlecock-like movement of non-axisymmetric chiral skyrmions *Sci. Rep.* **10** 1–9

[57] Kézsmárki I, Bordács S, Milde P, Neuber E, Eng L, White J, Rønnow H M, Dewhurst C, Mochizuki M and Yanai K 2015 Néel-type skyrmion lattice with confined orientation in the polar magnetic semiconductor GaV$_4$S$_8$ *Nat. Mater.* **14** 1116–22

[58] Zhao G P and Wang X L 2006 Nucleation, pinning, and coercivity in magnetic nanosystems: an analytical micromagnetic approach *Phys. Rev.* B **74** 012409

[59] Merzbacher E 1961 *Quantum Mechanics* (New York: Wiley)